Measurement and Modeling of Nonlinear Magnetic Core Characteristics of a Fluxgate Direct Current Sensor for Wide-Range Current Monitoring

Takafumi Koseki*, Yasuhiro Takada*, Hiroshi Obata*,Yori Hayakeyama**, Wolfram Teppan**, Eric Favre**
* Department of Electrical Engineering, School of Engineering, The University of Tokyo, Japan
** LEM-Japan, Japan and LEM SA, Switzerland, respectively

***Abstract*--Fluxgate sensors are the most sensitive and reliable ones among different kinds of current sensors used in normal temperature. The sensor can measure a few milliamperes direct current. It is, therefore, applied in various small current measurements, especially for battery monitors. This paper proposes the way for extending current measurement range to a hundred amperes by using the information of secondary excitation frequency. The authors derive the dynamic circuit equations for analysing the frequency characteristics and a method for identify the nonlinear magnetic characteristics of the ferromagnetic core to the primary current.**

***Keywords*--fluxgate sensor, battery monitoring, nonlinear magnetic core, current sensor**

I. INTRODUCTION

Current sensors are used widely in the control and observation of countless electronic products, testing for the stability of current flows and loss in the system, thus, the study has high commercial importance. Among them, the fluxgate current sensor is a highly sensitive current sensor for the testing of DC and is used at room temperatures as shown in Fig. 1. Its simplicity and durability in design gives it high commercial values. The fluxgate sensor was traditionally designed and used in the sensing of changes in magnetic fields but is gradually used as a technology in DC sensing. A single-core fluxgate current sensor consists fundamentally of a soft magnetic core, a coil for generating high amplitude magnetic signal as well as to test for the change in magnetic flux density. Also, the fluxgate sensor is made up of an element that practically senses the magnetic field induced by the primary current to be tested and an electric circuit which drives the element to operate as a current sensor. In general, the fluxgate technology offers the following advantages:

(1) Low offset and offset drift, because the magnetic core is cycled through its hysteresis loop, suppressing any magnetic offset in the fluxgate core.

(2) Excellent accuracy: Compared to Hall based technologies, this advantage is more noticeable for small current measurement, where the relative effect of the offset is more significant. And

(3) Large temperature range, the low offset drift makes fluxgate technologies suitable for broad operation ranges. The technology has in general the following limitations:

(1) The requirement of an external power source, and

(2) a small dynamic range.

A new technology allowing measurement of both small and large currents with the same transducer is required when we apply the sensor to battery monitors shown in Fig. 2, whose leakage current is small whereas the load current can be more than a hundred amperes. This paper proposes a new method for solving the problem 2. The information on nonlinear magnetic curve of a core is significant for a novel mode of large current monitoring.

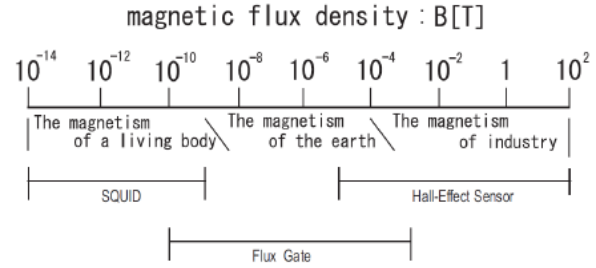

Fig. 1 Detectable magnetic field range for various types of sensors.

Fig. 2 Battery monitoring system.

II. Principle of Fluxgate Current Sensor

The fluxgate sensor[1] is used in the sensing of magnetic fields or electric currents, which operates on sudden drops in the non-linearity of the magnetic permeability of highly magnetic bodies near magnetic flux saturation. The structure of the fluxgate model used in the study is shown in Fig. 3. It consists of a magnetic core in the form of a ring, a coil which supplies the drive voltage and picks up changes in current signal due to the primary current to be tested, I_e, which flows through the centre of the ring.

From the circuit model of the fluxgate sensor in Fig. 4, the following magnetic equations (1), (2), and (3) are obtained.

$$e(t) = RI(t) + N\frac{d\Phi(t)}{dt} = RI(t) + NS\frac{dB(t)}{dt} \quad (1)$$

$$2\pi r H(t) = NI(t) + I_e(+N_{cancel}I_{cancel}) \quad (2)$$

$$H(t) \approx H_0(t) + \frac{dH}{dB}\Delta B(t) \quad (3)$$

Fig. 5 shows an example of an industrial products of the fluxgate sensors supplied by LEM[2].

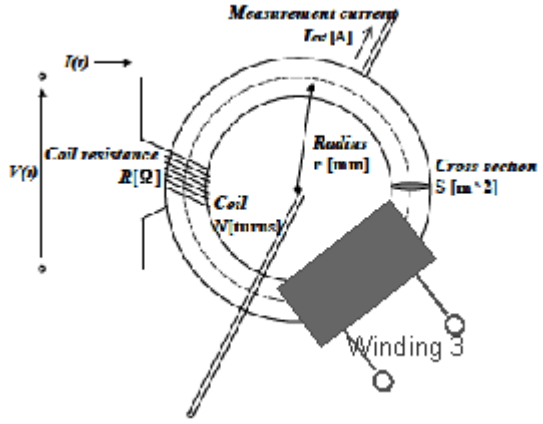

Fig. 3 The structure of a fluxgate current sensor/

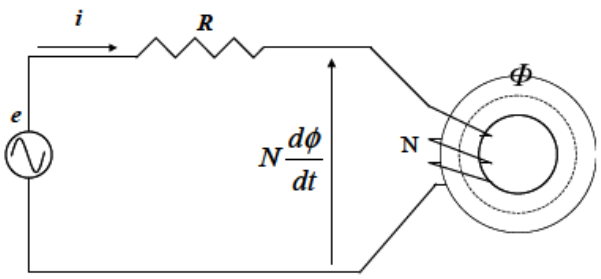

Fig. 4 Magnetic and electric circuits

A. Conventional Fine direct current measurement: Mode I

A threshold current level is added to the step signal of the drive voltage so that it switches its sign when the magnetic core reaches saturation. The change in magnetic flux density is integrated in the dynamics of the sensor, and the signal is superposed with the primary current I_e, generates the internal current of the sensor, I. This internal current feedbacks to the drive voltage which operates according to the threshold current level dictated by the internal current.

The drive voltage used in the model is a square wave, the corresponding output current in the presence of a DC input component is shown in Fig. 6. When $I_e = 0$, the output current balances in the positive and negative region. But when $I_e > 0$, the magnetic flux generated by I_e is in the same direction as the flux generated by the output current, as a result of the overlapping in flux change, the positive pulse reaches saturation earlier than the negative pulse. When $I_e < 0$, the opposite occurs.

By setting the drive voltage to switch its sign in the critical value when the magnetic core reaches saturation by the application of a threshold current level, the difference in speed for the pulses to reach saturation is expressed by the time needed for the positive and negative pulses to reach saturation, as in Fig. 7, this change is linearly proportional to the change in I_e.

For an actual commercial sensor as in Fig. 5, the acquirement of the internal current signal is more practical than the extraction of the drive voltage signal, this current signal is converted to a voltage signal by passing it through a resistor and then a low pass filter and the result is linearly related to I_e, thus the working of the fluxgate current sensor for DC analysis.

The linearity shown in Fig. 7 is obtained just in small I_e-range, *i.e.*, from -2 to +2 A in the example. Therefore, it cannot be used for load current measurement in battery monitoring system as shown in Fig. 2, although it may be appropriate for leakage current detection when external load is off.

We define this operational mode as Mode I.

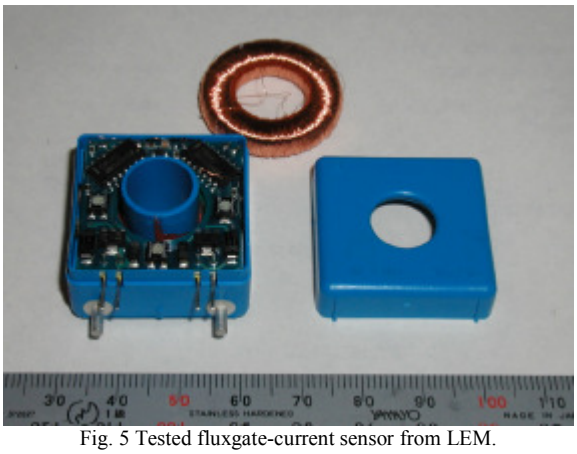

Fig. 5 Tested fluxgate-current sensor from LEM.

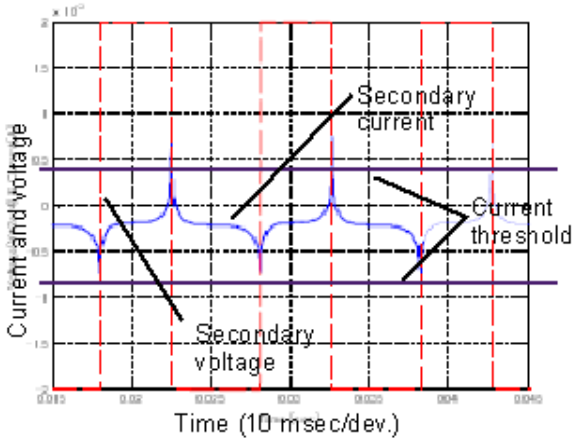

Fig. 6 Rectangular secondary excitation voltage waveform and secondary current.

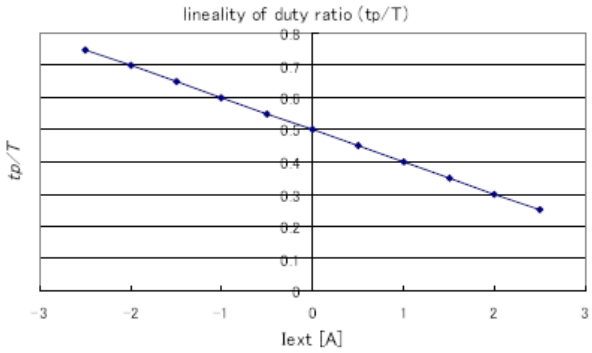

Fig. 7 measured primary current and duty ration of the secondary circuit.

B. Possible ways of extending current measurement range

In order to use the sensor for monitoring large load current, the following two methods based on its single-core structure are possible.

1) Equilibrium method using an additional canceling winding

If you set the third winding around the core as illustrated in Fig. 3 and apply appropriate negative current for canceling the core flux from large I_e, the magnetic operating point on the *BH*-curve of the core is identical to the Mode I. The advantage of this method is that you can just apply the same process for knowing the primary current I_e if you know the amount of the canceling current I_{cancel} in (2) and the measurement is as accurate as Mode I in principle. But it maybe an expensive solution, since it requires the third winding, additional current source and its controller to cancel the external primary current I_e, and additional electronic components for identifying I_{cancel}.

2) Measurement of secondary excitation frequency depending on the primary direct current

The Mode I uses the asymmetry of the rising times in positive and negative directions of the secondary current caused by partial core saturation. When the core is saturated, the inductance of the secondary winding is drastically reduced and the time constant of the secondary current is, consequently, reduced, since the time constant $T = \frac{L}{R}$. When the core is furthermore saturated by the larger contribution of the primary current I_e, the frequency of the secondary excitation square-wave voltage $e(t)$ is increased by the smaller $T = \frac{L}{R}$. We will define this operating process as Mode II.

Fig. 8 shows empirical data of the excitation frequency dependent on the external primary current I_e, and the operating ranges of Modes I and II. Although the operation in Mode II directly depends on the analogue nonlinear property of the magnetic core and cannot be accurate, it may be much more preferable and cheaper solution to the request of coarse monitoring of large load current without any additional components except for a frequency-voltage converter.

Fig. 9 shows measured secondary current and voltage waveforms in the case of $I_e = 0$ in Mode I

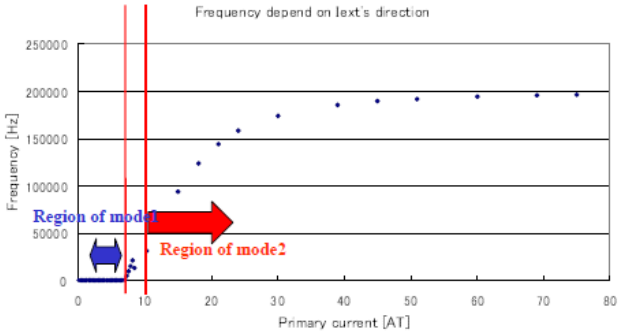

Fig. 8 Secondary excitation frequency and the definition of Mode 1 and Mode II

III. Analysis of the Dynamic Behaviour

In addition to the equations (1)-(3),

$$\frac{dB(t)}{dt} = \frac{dB(t)}{dH(t)} \bullet \frac{dH(t)}{dt} \qquad (4)\,.$$

The time differential of (2) is

$$\frac{dH(t)}{dt} = \frac{1}{2\pi r}\left(N\frac{dI(t)}{dt} + \frac{dI_e}{dt}\right) \qquad (5).$$

When (4) and (5) are substituted into (1),

$$\frac{dI(t)}{dt} = \frac{2\pi r}{N^2 S}\left(e(t) - RI(t)\right)\frac{dH(t)}{dB(t)} \qquad (6).$$

For dynamic calculations, equations (1) and (6) are mainly solved. By applying variational linear-approximation in (3) and state space representation, the dynamic equation of the secondary current (6) is calculated by using transition matrix of a state equation[1]. Obviously, empirical data of the gradient of the magnetic curve of the core $\frac{dB(t)}{dH(t)}$ are important for calculating secondary current waveform from (6).

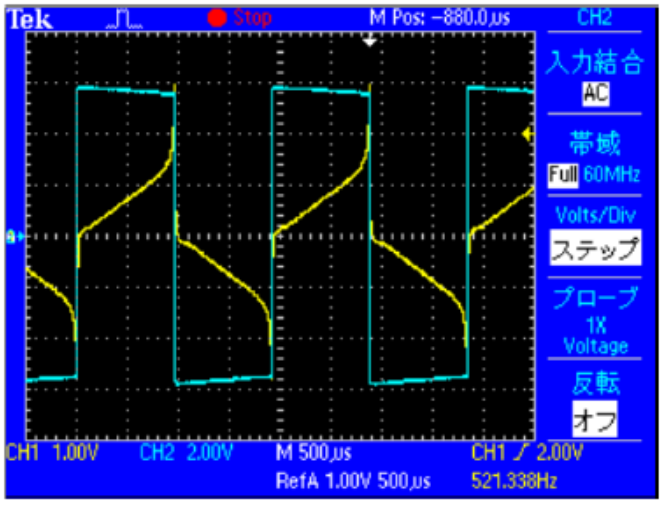

Fig. 9 Measured secondary current and voltage waveforms at I_e = 0 A.

IV. Measurement of Nonlinear Characteristics of the Core

For the dynamic calculation of the secondary *VI*-characteristics useful for sensor design, efficient and exact identification of the nonlinear magnetic characteristics is important. Therefore, the voltage and current characteristics of the secondary winding were measured with different I_e's by using the circuit in Fig. 10. The current is calculated from the voltage V_R of the series-connected resistance R_0 : $I(t) = \frac{V_R}{R_0}$. The magnetic intensity *H(t)* is calculated from (2), *i.e.*,

$$H(t) = \frac{1}{2\pi r}\left(Ni(t) + I_e\right) \qquad (7).$$

Fig. 11 shows how to apply large primary current in the experiment. Fig 12 (a) shows an example of measured waveforms of V_R and V_L.

The magnetic flux density *B(t)* is not directly measured, but by integrating (8), it is calculated in (9), where *C* is the integral constant.

$$\frac{dB}{dt} = \frac{V_L(t) - R_{in}V_R(t)}{NS} \qquad (8)$$

$$B = \int \frac{dB}{dt}dt + C \qquad (9)$$

By plotting the results calculated from (7) and (9) by giving $C = 0$, the *BH*-trajectory for a given I_e can be drawn as shown in Fig. 12 (b). Although the absolute value of the flux density is not determined uniquely, the average value of $\frac{dB}{dH}$, which is significant for the dynamic analysis, is calculated from Fig. 13. By changing the primary currents and repeating the measurements, the $\frac{dB}{dH} - I_e$ characteristic curve is obtained as shown in Fig. 14.

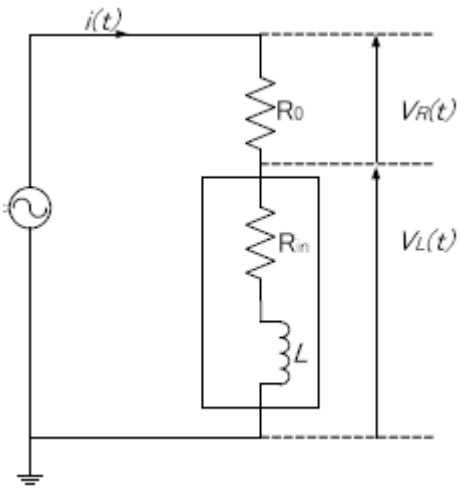

Fig. 10 Circuit for measuring secondary impedance and magnetization characteristics of the ferromagnetic core.

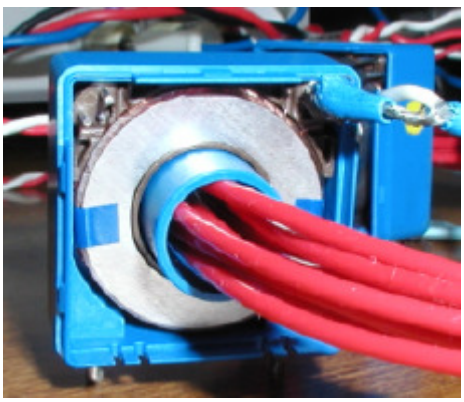

Fig. 11 Sensor head with large primary ampere turns.

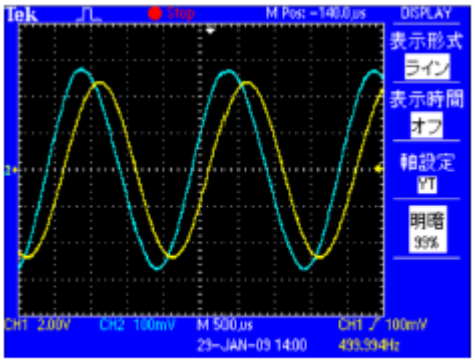

(a)Experimental data (V_H:yellow, V_L:blue)

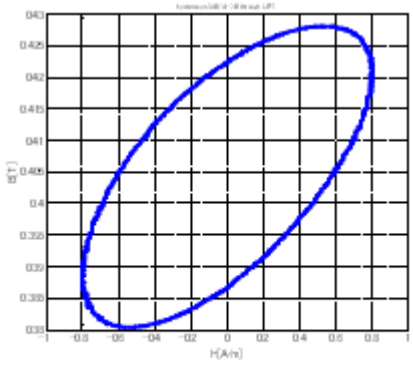

(b)Hysteresis curve (I_{ext}=0 [AT])

Fig. 12 Empirical data at V_{pp} = 10 V.

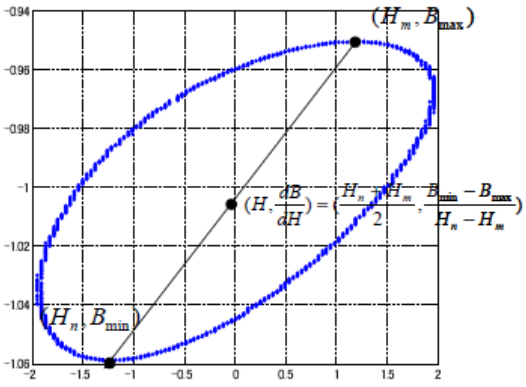

Fig. 13 Empirical calculation of *H* and *dB/dH*.

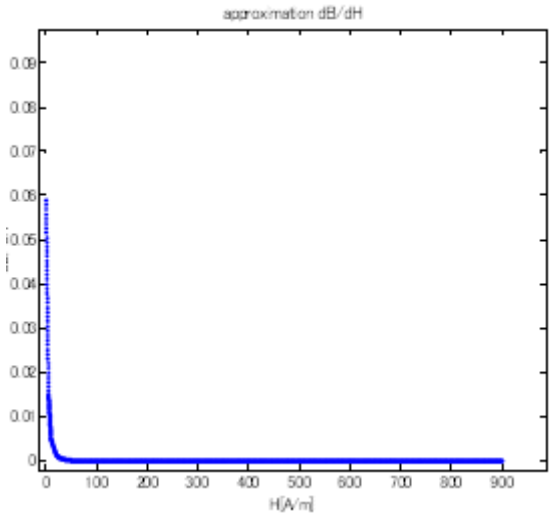

Fig. 14 Empirical dB/dH data calculated as shown in Fig. 13.

By using the results of nonlinear $\frac{dB}{dH}$ characteristics in Fig. 14 and calculating the secondary current by solving the dynamic equation (6), the secondary frequency depending on the primary current I_e has been calculated.

An calculated result based on Fig. 14 is shown in Fig. 15. The secondary excitation frequency at large I_e in Fig. 15 is larger than the measured characteristics in Fig. 8. The current and voltage waveforms at $I_e = 80$ A in Fig. 8 is shown in Fig. 16. In spite that the secondary excitation voltage in Fig. 9 is square waveform, the voltage in Fig. 16 seems trapezoidal waveform. Since the time-constant of the secondary winding in such highly saturated cases is too small, and the consequent secondary excitation frequency is too high, the operation in Mode II was beyond dynamic frequency range of the electronic circuit for driving the secondary excitation voltage. Therefore the frequency characteristics in Fig. 8 were determined by the upper limit of the speed of the secondary driver circuit, and were lower than the excitation frequency expected from nonlinearity of the magnetic circuit assuming ideal driver electronic circuit. Even though the empirical results in Fig. 8 were not in good agreement with the theoretical analysis in Fig. 13, it may be still useful for coarse load current monitoring in practice, since the resultant frequency characteristics containing the response limitation of the driver-circuit can be identified uniquely by preliminary calibration process.

However, for guaranteing accuracy of the primary current measurement, it is strongly recommended to do the preliminary identification of $\frac{dB}{dH}$ described in this chapter and calculate the expected maximal secondary frequency shown in Fig. 15. And redesign the secondary driver electronic circuit which allow the square waveform

drive at the maximal frequency.

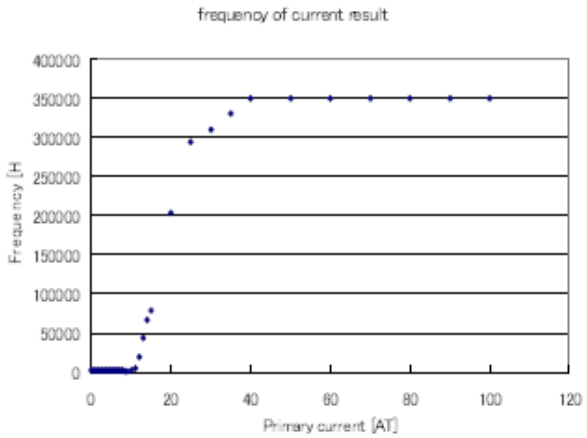

Fig. 15 Secondary current frequency vs. Primary current calculated based on the *dB/dH* data in Fig. 14

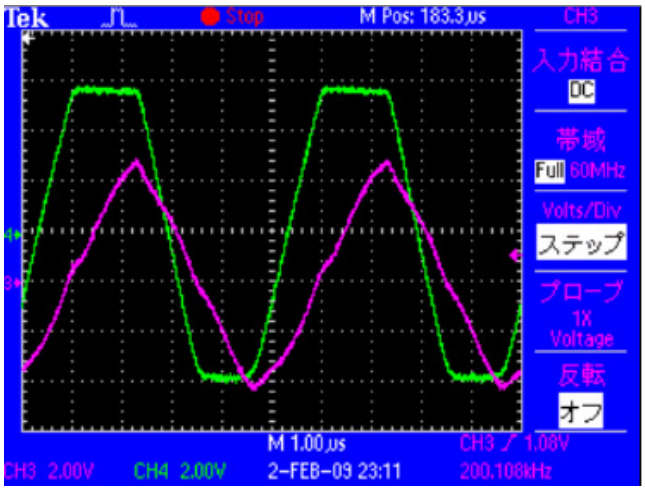

Fig. 16 Measured secondary current and voltage waveforms at I_e = 80 A.

V. Conclusions

This paper has proposed to use information of the frequency of the secondary excitation voltage of the fluxgate direct current sensor for coarse measurements of substantially larger external primary current. This extension of the fluxgate current sensor, which was originally designed for accurate measurement of small external current, is possible just by adding simple *f/V*-converter to the existing fluxgate current sensor and an additional simple calibration process for drawing secondary frequency-primary current characteristic curve in the proposed Mode II. Fundamental dynamic circuit equation of the secondary winding has been derived and the method for calculating the secondary frequency-primary current characteristics has been concretely described. An efficient and reliable method for identifying nonlinear $\frac{dB}{dH} - I_e$ characteristics has been established and described.

The response of the secondary excitation driver circuit was too slow in the proposed Mode II, *i.e.*, in highly saturated cases, and the frequencies of the empirical data were much lower than the theoretical expectation. For a really reliable realization of the measurement in Mode II, the upgraded redesign of the secondary driver circuit is desired. However, even with the existing slow driver circuit, the extension of the current measurement range based on the proposed idea is still available by calibrating resultant frequency characteristic curve, which contains non-ideal frequency response of the driver circuit.

Since the proposed measurement method in Mode II is directly sensitive to the change of the analogue property of the ferromagnetic core and winding circuit, sensitivity analysis to temperature changes and external magnetic field shall be furthermore studied.

Nomenclature

$e(t)$: Secondary excitation voltage

R , R_{in} : Resistance of the secondary winding

$i(t)$, $I(t)$: Secondary current

$\Phi(t)$: Core flux

N : Secondary winding number

S : Core cross-section

r : Core ring radius

$H(t)$: Magnetic intensity

$B(t)$: Core magnetic flux density

I_{ext} , I_e : External primary direct current

N_{cancel} : Winding number of the third virtual winding

I_{cancel} : Canceling current in the third winding

References

[1] E. Hashiguchi, T. Koseki, E. Favre and M. Ashiya and T. Tachibana:"Non-linear magnetic circuit analysis of fluxgate current sensor," 12th International Symposium on Interdisciplinary Electromagnetic, Mechanic and Biomedical Problems, short paper proceedings, pp. 76-77, September 2005

[2] LEM "Isolated current and voltage transducers -- Characteristics --Applications --Calculations", 3rd Edition